ICARUS 118, 341–354 (1995)

Ejection Velocity of Ice Impact Fragments

MASAHIKO ARAKAWA, NORIKAZU MAENO, AND MICHIYA HIGA

Institute of Low Temperature Science, Hokkaido University, Kita-ku Kita-19 Nishi-8, Sapporo 060, Japan
E-mail: arak@orange.lowtem.hokudai.ac.jp

AND

YU-ICHI IIJIMA AND MANABU KATO

Department of Earth and Planetary Science, Nagoya University, Nagoya 464-01, Japan

Received January 23, 1995; revised June 12, 1995

Laboratory experiments on the impact disruption of ice were carried out to investigate the collisional phenomena of an icy planet. Ice projectiles were impacted on ice targets at impact velocities of 30 to 530 m/sec, and mass ratios of the projectile to the target of 0.1 to 0.0035. An ejection velocity at an antipodal point (V_a) and a largest-fragment mass normalized by the target mass (m_l/M_t) were used to examine two scaling parameters, an energy density (Q) and a nondimensional impact stress (P_I). The largest-fragment mass and the antipodal velocity have good correlations to Q but show apparent differences from a basalt target obtained by previous studies. The ice target begins to break up at 83 J/kg, which is two to five times smaller than for basalt. The ejection velocity is about two times higher than for basalt at the same Q. A modified nondimensional impact stress, P_I^*, that involves a variable decay constant depending on the impact pressure is suggested. This eliminates the size dependence in the relation between P_I and the largest fragment. If we assume a simple relation to the antipodal velocity, $V_a/V^* = 2P_I^*$, where V^* is a characteristic velocity, the decay constant decreases with increasing impact velocity. The revised P_I^* improved the relation between m_l/M_t and the nondimensional impact stress. Ejection velocity in a center-of-mass frame was used to estimate a collisional condition for the icy planet to reaccumulate the disrupted fragments by planetary gravity.

1. INTRODUCTION

The velocity measurement of impact fragments is necessary in studies of kinematic collision processes in the solar system. The accretional growth process of a planet in the solar nebula was recently studied by Barge and Pellat (1993), Wetherill and Stewart (1993), and Hayakawa *et al.* (1989) in a model of the impact disruption. The origin of asteroids and asteroidal families could be closely related to the impact disruption of the parent bodies and to the ejection of the fragments away from the gravitational field of the planet. Velocity observations of ejecting fragments were made by Fujiwara and Tsukamoto (1980), Takagi (1983), and Waza *et al.* (1985) for basalt, and by Davis and Ryan (1990) for mortar with various strengths. They found a power-law relation between the ejection velocity at an antipodal point and the energy density or a nondimensional impact stress. Nakamura and Fujiwara (1991) and Nakamura *et al.* (1992) tried to measure 3-D velocity and spin rate of the fragments and obtained the velocity distribution of the fragments for basalt and alumina spherical targets.

Ice is the most abundant material in the outer solar system and many icy satellites were found to have impact features on their surfaces, as revealed by Voyager spacecraft, so the origin and the evolution of the giant planets and the icy satellites must have a close relation to the collisional process of icy planetesimals. The impact fragmentation experiments for ice were carried out by Kawakami *et al.* (1983), Lange and Ahrens (1983, 1987), Cintala *et al.* (1985), and Kato *et al.* (1992, 1995); they clarified the characteristics of the largest-fragment mass and the mass distribution of the ice fragments. However, no study of the velocity distribution of the ice fragments has been made, so we made experiments to measure the ejection velocity at the antipodal point by ice-to-ice impact at −18°C. The velocity and the mass ratio were changed over a wide range in order to examine the proposed scaling parameters. The material dependence of the ejection velocity and the applicability of the scaling parameter were clarified. The condition for the planets to capture the collisional fragments by gravity was also discussed on the basis of our new data and the revised scaling parameters.

0019-1035/95 $12.00

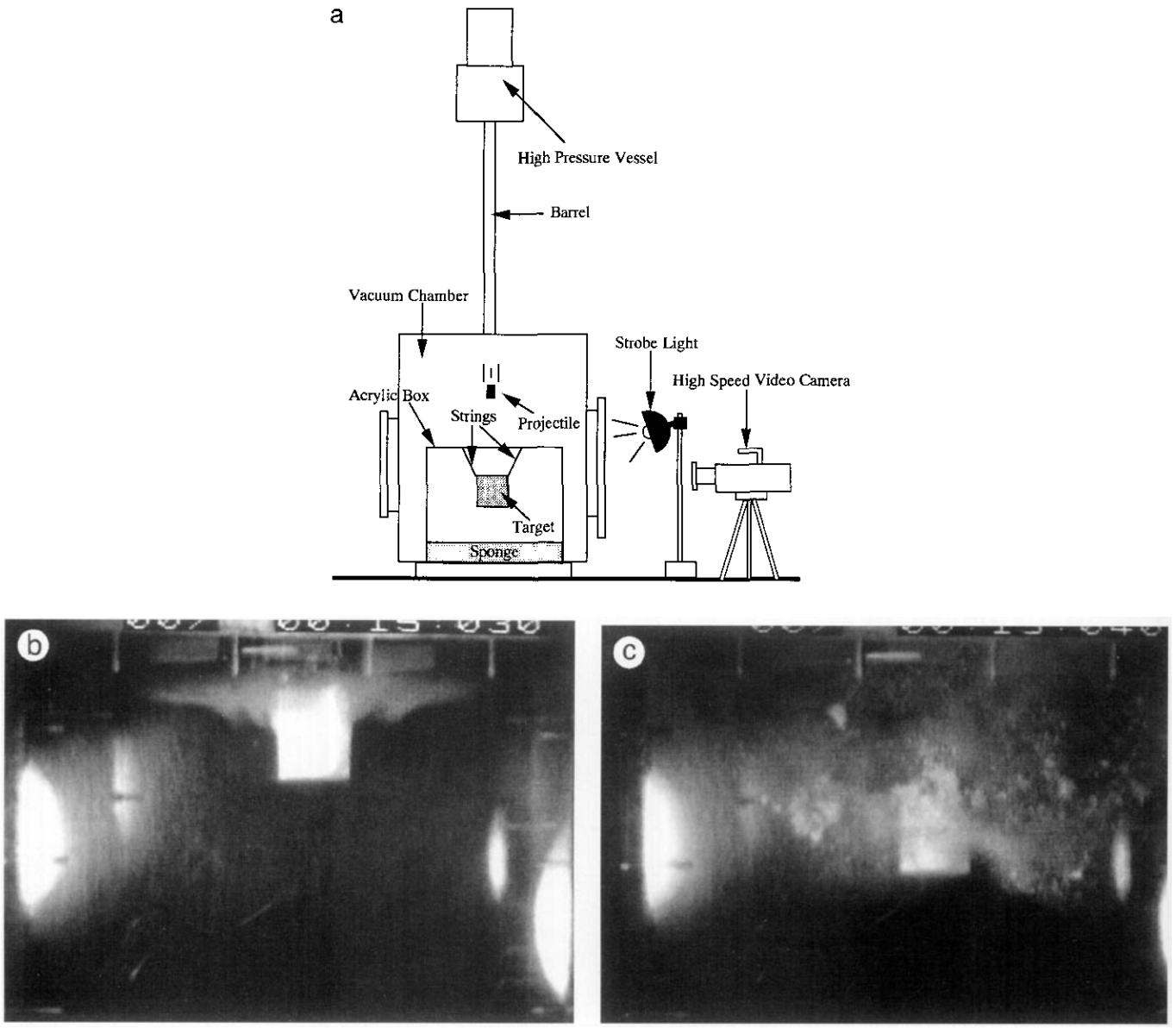

FIG. 1. (a) Schematic figure of the experimental apparatus. Recorded snapshots of a disrupting ice target (Cy 6) are shown in Fig. 1b and Fig. 1c. (b) Image recorded within 5 msec after the impact. (c) Image recorded 10 msec after the image (b). White circular objects at left and right sides are the mirror images of stroboscopic light on the acrylic box.

2. IMPACT EXPERIMENTS

A clear, polycrystalline ice commercially delivered was used for this experiment, which consists of columnar ($1 \times 1 \times 10$ cm^3) crystals elongating toward a crystallographic *a*-axis. Two types of targets, cubic and cylindrical, were prepared for studying any shape effect. These targets were made by cutting the ice block ($30 \times 50 \times 100$ cm^3) with a band saw and a lathe. The sizes of the cubic targets were from 3 to 10 cm in edge length, and those of the cylinder targets were 3.6×3.6, 4.5×4.5, 5.6×5.6 cm in diameter and height, respectively. Thus, the targets were composed of several ice crystals. An ice cylinder (diameter 15 mm, height 20 mm, 3.2 g), which was made from water cooled in an aluminum mold at −18°C, was used as a projectile.

High-velocity impact experiments were made by using a single-stage vertical light-gas gun, which has a 1-m barrel length and a 15-mm bore (Fig. 1a) (Kato *et al.* 1995). A large cylindrical chamber (diameter 0.7 m, height 1 m) was set under this gun barrel for target recovery and was evacuated before firing. The light-gas gun uses high-

pressure helium gas to accelerate an ice projectile set at the entrance of the gun barrel. This gun was able to accelerate a projectile with a mass of 1.7 g up to 900 m/sec in a cold room where the temperature was maintained at −18°C. The projectile velocity was measured by a laser-beam system installed in the chamber. A transparent box (50 × 50 × 50 cm^3) of acrylic resin set in the chamber was used for recovering ice fragments in a collisional disruption. Ice targets were hung with strings in the transparent box and a sponge shock-absorber with 5 cm thickness was set on the base of the box to prevent fragments from breaking by colliding with the box walls. As the strings were weakly attached at the four corners of the sample, they hardly influenced the behavior of the target. The experimental conditions and results are listed in Table I. The impact velocity (V_i) ranged from 30 to 530 m/sec and the mass ratio of projectile to target (m_p/M_t) was 0.1 to 0.0035. All the impact experiments were designed to make the projectile collide with the front center of the target surface (head-on collision).

The ejection velocity of fragments at the antipodal point (V_a) was measured in a two-dimensional frame by using a high-speed video camera. This camera (NAC HSV-200) can record pictures at 200 frames/sec; the shutter speed was 5 msec and the flashing time of the stroboscopic light was about 20 μsec. The maximum velocity which could be measured in this system was about 30 m/sec because the observational area of fragments was roughly 20 × 20 cm. Although the recorded picture was a superimposed image during the flushing time of 20 μsec, this duration was short enough for the ejecting fragments to be taken as a still image. The fragment ejected from the antipodal point could be observed clearly because fragments near the rear edge could be easily distinguished from the surroundings (Figs. 1b and 1c). It was difficult to measure the velocities of other fragments because they had higher ejection velocities and fine sizes. In this head-on collision the fragments near the antipodal point ejected toward the impact direction of the projectile without any other velocity components; thus, the velocities in a two-dimensional frame can be regarded as three-dimensional. The video images of the second, third, and fourth frames after the collision were used for determining the ejection velocity and the mean ejecting velocity was estimated as 10 msec. The positions of the antipodal fragments were measured on the video monitor. The spatial resolution of the monitor was about 1 mm, so the error of velocity measurements was within 0.2 m/sec. The gravitational acceleration effect on the fragment velocity was considered in this analysis, its correction value was 0.05 m/sec for 5 msec. After the impact experiment, all the recovered fragments heavier than 0.1 g were weighed by an electronic balance in the cold room to determine the largest-fragment mass.

3. SCALING PARAMETERS

We used two key parameters to analyze our experimental results, the energy density Q and the nondimensional impact stress (NDIS) P_I. The former parameter is defined as the ratio of projectile kinetic energy to target mass ($\frac{1}{2} V_i^2 (m_p/M_t)$). The latter parameter, which was proposed by Mizutani *et al.* (1990) on the basis of generation and propagation of a shock wave through a solid material, was defined as the ratio of impact pressure at the antipodal point in the target to material strength. Mizutani *et al.* suggested that the difference in material between projectile and target and the difference in sizes and impact velocities would induce a difference in the stress distribution generated in the targets. Thus, the degree of fragmentation could be controlled by a suitable key parameter P_I, which is defined as

$$P_I = \frac{P(L_t)}{Y_t} \tag{1}$$

and

$$P(L_t) = P_0 \left(\frac{L_p}{L_t}\right)^{\alpha}, \tag{2}$$

where α is the decay constant of the impact pressure, Y_t is the material strength, L_p and L_t are the sizes of the projectile and the target, and P_0 is the impact pressure at the collision point. When the materials are the same, Eq. (2) can be approximated by $P(L_t) = P_0 (m_p/M_t)^{\alpha/3}$. The compressive strength of ice, 70 MPa, determined by Arakawa and Maeno (1992) was adopted for Y_t here, because the tensile strength of ice for a wide strain rate and temperature range is not clarified yet; thus, use of the compressive strength is more practical. The decay constant of the shock wave α for ice is uncertain and probably ranges from 1.5 to 4.5 (Kieffer and Simonds 1980, Melosh 1989), although α was 3, according to Mizutani *et al.* The impact pressure at the collision point P_0 was estimated using experimental data at a low impact velocity by Larson (1984) and Gaffney (1985). At particle velocities lower than 100 m/sec, the pressure is approximately written as

$$P = \rho_0 C_b u_p, \tag{3}$$

where ρ_0 is the initial density (917 kg/mec^3), C_b is the bulk sound velocity of 3110 m/sec (Gold 1958), and u_p is the particle velocity. The ejection velocity at the antipodal point for spall fragments was theoretically estimated by Rinehart (1975). From theoretical considerations, Mizu-

TABLE I
Experimental Conditions and Results

Run No.	V_i m/s	M_t g	Q J/kg	V_a m/s	V_a/V^*	m_l/M_t	P_I	n	P_I^*
Cu1	48.3	25.98	144	4.54	0.185	0.988	0.142	(1.20)	(0.093)
Cu2	32.9	30.62	56.6	3.05	0.124	0.837	0.083	(1.13)	(0.062)
Cy1	50.2	32.45	124	4.30	0.176	1.00	0.118	(1.13)	(0.088)
Cu3	71.9	24.68	335	7.52	0.307	0.895	0.218	(1.17)	(0.153)
Cu4	70.0	30.85	254	6.27	0.256	0.222	0.170	(1.13)	(0.128)
Cy2	38.8	34.36	106	4.36	0.184	0.915	0.123	(1.14)	(0.092)
Cy3	72.6	62.42	135	3.80	0.155	0.905	0.087	(1.04)	(0.078)
Cy4	59.5	135.35	41.9	1.62	0.066	1.00	0.033	(1.00)	(0.033)
Cu5	111	25.74	766	15.64	0.638	0.054	0.311	0.99	0.319
Cu6	95.2	26.03	557	10.25	0.418	0.053	0.268	1.12	0.209
Cu7	105	28.35	617	9.22	0.376	0.144	0.268	(1.16)	(0.188)
Cy5	98.4	33.98	456	8.20	0.335	0.032	0.211	1.10	0.167
Cu8	107	61.51	298	5.08	0.207	0.069	0.126	1.07	0.104
Cy6	108	67.82	275	5.00	0.204	0.239	0.115	(1.04)	(0.102)
Cu9	110	121.22	160	3.28	0.134	0.229	0.066	(0.99)	(0.067)
Cu10	110	121.22	160	2.88	0.118	0.188	0.066	(1.03)	(0.059)
Cy7	110	136.46	142	2.50	0.102	0.796	0.058	(1.04)	(0.051)
Cu11	106	233.96	76.8	1.29	0.053	1.00	0.033	(1.05)	(0.026)
Cu12	177	26.44	1900	21.71	0.886	0.005	0.454	1.01	0.443
Cu13	180	60.77	853	10.49	0.428	0.061	0.200	0.98	0.214
Cy8	187	68.21	820	9.30	0.380	0.028	0.184	0.99	0.190
Cu14	169	116.03	394	5.80	0.237	0.080	0.100	0.95	0.118
Cy9	186	134.38	412	6.10	0.249	0.676	0.093	(0.92)	(0.124)
Cy10	180	134.88	384	5.10	0.208	0.256	0.090	(0.96)	(0.104)
Cu15	177	241.76	207	4.02	0.164	0.353	0.0450	(0.88)	(0.0820)
Cu16	182	315.07	168	2.27	0.093	0.315	0.039	(0.96)	(0.0463)
Cu17	250	120.92	827	9.78	0.399	0.052	0.130	0.88	0.200
Cy11	245	135.34	710	...	...	0.106	0.115	...	...
Cu18	242	237.88	394	5.38	0.220	0.381	0.065	(0.88)	(0.110)
Cu19	250	315.65	317	4.20	0.171	0.098	0.050	0.88	0.086
Cu20	239	494.20	185	2.08	0.085	0.385	0.031	(0.94)	(0.042)
Cu21	256	634.09	165	2.19	0.089	0.677	0.025	(0.89)	(0.045)
Cu22	244	908.94	105	1.27	0.052	0.870	0.017	(0.93)	(0.026)
Cu23	350	110.14	1780	20.18	0.824	0.017	0.179	0.76	0.412
Cu24	352	241.76	820	9.98	0.407	0.027	0.082	0.79	0.204
Cu25	333	316.89	560	6.70	0.273	0.086	0.060	0.82	0.137
Cu26	336	908.00	199	2.70	0.110	0.118	0.021	(0.83)	(0.055)
Cu27	347	926.11	208	2.86	0.117	0.233	0.021	(0.82)	(0.058)
Cu28	410	308.57	872	11.50	0.469	0.039	0.067	0.73	0.235
Cu29	410	903.35	298	5.56	0.227	0.079	0.024	0.72	0.113
Cu30	532	922.62	491	9.38	0.383	0.047	0.026	0.64	0.191

$n \equiv \alpha/3$.

Cu and Cy in the column of Run No. mean the cube and cylinder targets, respectively. The values in the columns of n and P_I^* whose m_l/M_t are larger than 0.1 are put in parentheses because for large m_l/M_t the applicability of Eq. (11) is ambiguous.

tani *et al.* (1990) derived the relation between P_I and the normalized ejection velocity V_a/V^*

$$V_a/V^* = \bar{f} P_I, \tag{4}$$

where $\bar{f}$ is written by

$$\bar{f} = \frac{C_b}{2L_1} \int_0^{2L_1/C_b} f(t)\, dt, \tag{5}$$

and

$$V^* = \frac{Y_t}{\rho_0 C_b}, \tag{6}$$

where $f(t)$ is the normalized wave form of the impact pressure, L_1 the spall thickness, and V^* the characteristic velocity of 24.5 m/sec for ice. Our experimental results of ice collisions were analyzed with these parameters, Q and P_I hereafter.

4. EXPERIMENTAL RESULTS

4.1. Observation of Impact Disruption

Figures 1b and 1c show examples of snapshots (Cy 6) recorded by the high-speed video camera after the impact. The size of the target cylinder was 4.5 cm and the impact velocity was 108 m/sec. In the impact disruption, the largest-fragment mass normalized by the target mass (m_l/M_t) was used as a parameter showing the degree of fracturing (e.g., Fujiwara *et al.* 1977). In this impact the resultant largest-fragment mass was $m_l/M_t = 0.24$. The target appears as a white square in the center of this photograph (Fig. 1b), which was taken within 5 msec after the impact. Although the target was transparent before the impact, it became opaque as many cracks were generated by the impact. Fine particles produced by the disruption of both projectile and target spread out from the impact site and formed a haze around the surface. Figure 1c was taken 10 msec after Fig. 1b. In addition to the fine particles, many fragments of various sizes were formed and ejected from the impact site. The white haze in Fig. 1b grew outward with the velocity of several m/sec. In spite of the disturbance of the haze, the rear edge of the disrupted target could be seen very clearly in both photographs. The movement distance of the center on this edge was measured to calculate the antipodal velocity.

4.2. Largest-Fragment Mass

The relation between the largest-fragment mass (m_l/M_t) and the energy density (Q) is shown in Fig. 2 at constant mass ratios (m_p/M_t). The largest fragments decrease from 1 to 0.01 as the energy density increases from 100 to 1000 J/kg. It was found that there was no shape effect on the largest fragments between the cube and cylinder targets. The data points fall in a narrow band in spite of the large difference between the mass ratio and the impact velocity. This means that the largest fragments are dependent only on the energy density irrespective of the mass ratio and the impact velocity; in other words, the energy density can be a good scaling parameter for the fragments. The relation is estimated using a least-squares fit to the data:

$$\frac{m_l}{M_t} = 10^{2.6\pm0.3} Q^{-1.3\pm0.1}. \tag{7}$$

The slope for ice, -1.3, is similar to that for basalt, $-0.9 \sim -1.5$ (Fujiwara *et al.* 1977; Takagi *et al.* 1984). The ice target began to break beyond 83 J/kg in this ice–ice collision, while basalt, whose static compressive strength is approximately three to four times larger than that of ice, is known to begin to break at $160 \sim 430$ J/kg by previous studies. The experimental data on basalt derived by Takagi *et al.* (1984) and Fujiwara *et al.* (1977) are plotted in Fig. 2 for reference. It is found that the energy density of ice at the onset of fracture is two to five times smaller than the energy density of basalt. This ratio of the energy density is almost the same as the ratio between the static compressive strengths. This similarity might show the proportional relation between the static strength and the dynamic strength.

Another scaling parameter P_I is examined by the same quantity (m_l/M_t) in Fig. 3, where the value of P_I was calculated using Eqs. (1) and (2) with $\alpha = 3$. The data points for different mass ratios are clearly separated. At a certain mass ratio the fragment becomes smaller with increasing P_I and such a simple trend is found at each mass ratio. The slope of the trend is steeper for the smaller mass ratios.

The basalt begins to break at 3×10^{-2} of P_I irrespective of the mass ratio, according to the data obtained by Takagi *et al.* (1984), and this value is almost the same as that of ice at a mass ratio of 3.5×10^{-3}. As we changed the target size, but kept a constant projectile size, the target size is the only factor affecting the mass ratio. Thus, a larger ice target fragments at lower P_I than a smaller one. P_I at a constant m_l/M_t varies more than an order of magnitude in the mass ratio between 0.1 and 0.0035. Does this result show the size effect on the material strength? Housen and Holsapple (1990) showed a theoretical size effect on the impact strength; it varies with the size as $Y_t \propto R^{-3/8}$ for appropriate parameters, where R is the size of the target. The strength of the ice should change by a factor of 2, according to their theory, when the target mass varies by 2 orders of magnitude. This strength change is too small to explain the variation found in our results. The results with a smaller ice projectile (1.7 g) given by Kato *et al.* (1995) are plotted in this figure to examine in detail the effect of target size on the largest fragment. The value of $m_p/M_t = 0.0015$ was obtained for the constant target size

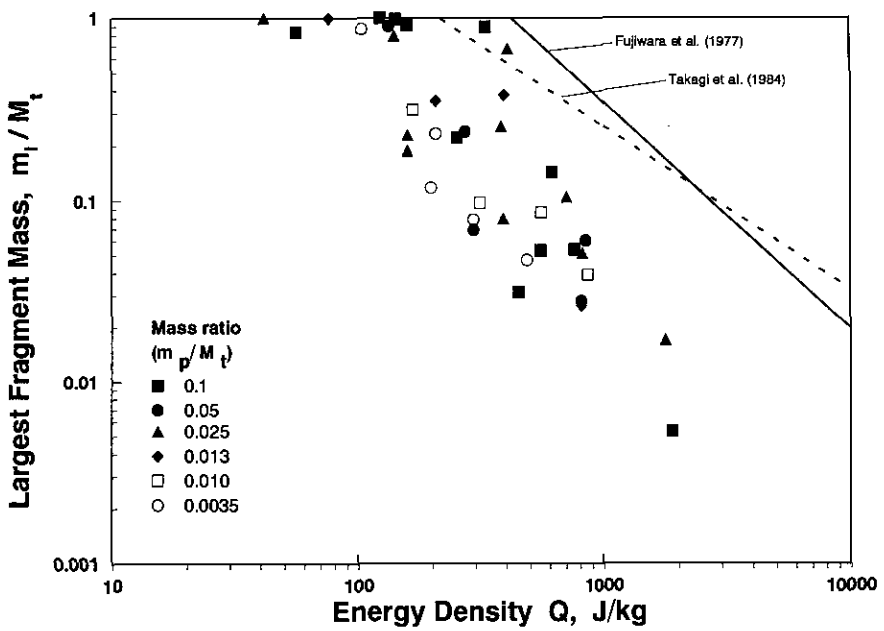

FIG. 2. Largest-fragment mass vs energy density for a constant mass ratio. Basalt data are given for reference by the solid line (Fujiwara *et al.* 1977) and the dashed line (Takagi *et al.* 1984).

of M_t = 900 g, which was the same size as our data for m_p/M_t = 0.0035. Although both results were obtained by the same target-size experiments, they are clearly separate from each other in this figure. This comparison suggests that the power-law dependence of target size on the strength is not primarily responsible for the mass-ratio dependence of the largest fragment. Thus P_I might be an insufficient parameter for describing impact fragmenta-

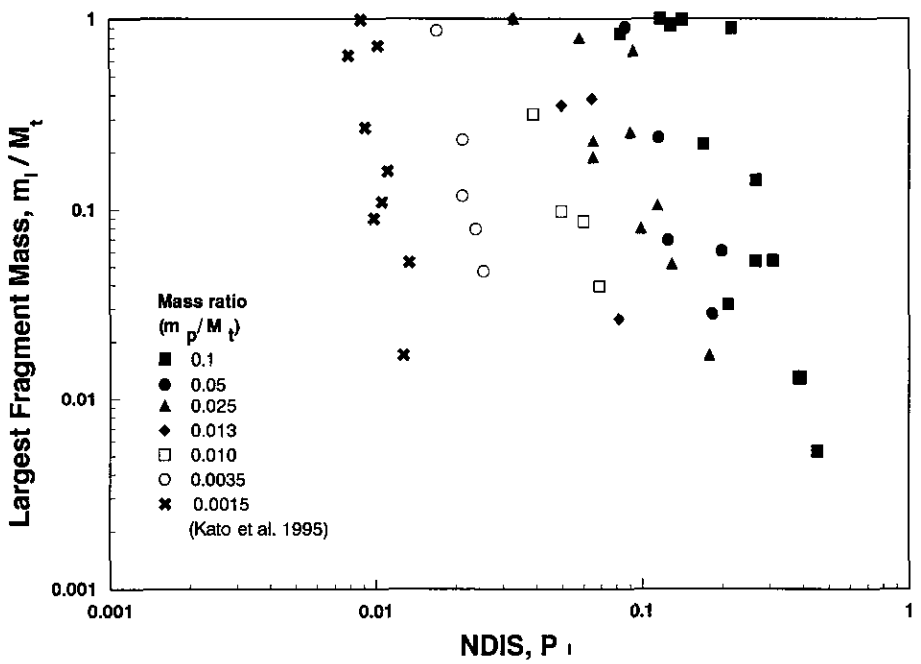

FIG. 3. Largest-fragment mass vs nondimensional impact stress at a constant mass ratio. P_I is calculated by Eqs. (1) and (2) with α = 3. The data for the smallest mass ratio (0.0015) obtained by Kato *et al.* (1995) with the impact of a small ice projectile (1.7 g) are also plotted.

tion. The pressure decay constant α in the definition of P_I is not an accurately determined value. It has a large ambiguity (1.5 ~ 4.5) (Kieffer and Simonds 1980, Melosh 1989), so we should reconsider the constant.

4.3. *Antipodal Velocity*

Figure 4 shows the relation between the ejection velocity at an antipodal point and the energy density for constant mass ratios. A velocity in a laboratory framework is used as it is usually convenient for us to treat the raw data, while a velocity in a center-of-mass framework is useful for the collision among planets with gravity. The ejection velocity increased from 1 to 20 m/sec as the energy density increased from 40 to 2000 J/kg. Rather good correlation is found at energy densities higher than 100 J/kg. Thus, the following relation is applicable above 100 J/kg;

$$V_a = 10^{-1.1\pm0.1} Q^{0.73\pm0.05}. \quad (8)$$

Detailed analysis of the data for each constant mass ratio shows significant differences in slope and intercept of fits to the data. The slope increases from 0.6 to 1.3 and the intercept decreases from 0.25 to 0.0025 with increasing mass ratio from 0.1 to 0.0035. When the ejection velocity of ice is compared with that of basalt using the equation

$$V_a = 3.51 \times 10^{-2} Q^{0.76}, \quad (9)$$

for basalt (Fujiwara and Tsukamoto 1980), ice has twice the velocity at the same energy density: 6.7 m/sec for basalt and 12.3 m/sec for ice at 1000 J/kg. It is difficult to explain why this material dependence was generated. A pressure attenuation and the fracture strength of both materials might be responsible for the difference.

Equation (4) theoretically predicts a linear relation between V_a/V^* and P_I. This relation for our data is examined in Fig. 5 for constant impact velocities. It can be seen that the normalized ejection velocity does not increase as a linear function of P_I, but as a power law relation $V_a/V^* = aP_I^b$. The relations are plotted in the figure for each impact velocity. This figure shows that the relation at higher impact velocities gradually moves upward with increasing impact velocity except for the velocity data at 60 and 100 m/sec, which are almost the same. The power index b is almost constant, 0.87 ($\pm$0.11), irrespective of the impact velocity, and is close to the predicted value of 1, while a varies between 1.0 and 4.0 with V_i. The data for the antipodal velocity of basalt compiled by Mizutani *et al.* (1990) showed that b was almost constant between 0.96 and 1.00.

The constant a obtained by Takagi (1983) was 4.4, which is nearly twice as large as the value of 2.5 obtained by Fujiwara and Tsukamoto (1980), but these values are within our values obtained for ice. The constant a corre-

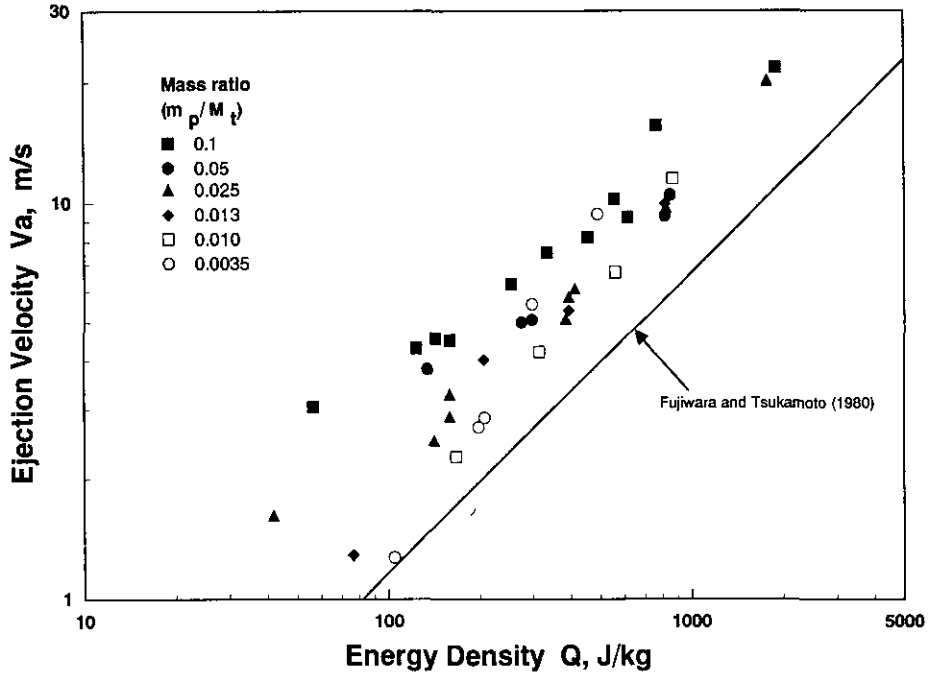

FIG. 4. Ejection velocity at the antipodal point vs energy density at a constant mass ratio. The antipodal velocity for basalt (Fujiwara and Tsukamoto 1980) is also plotted for reference.

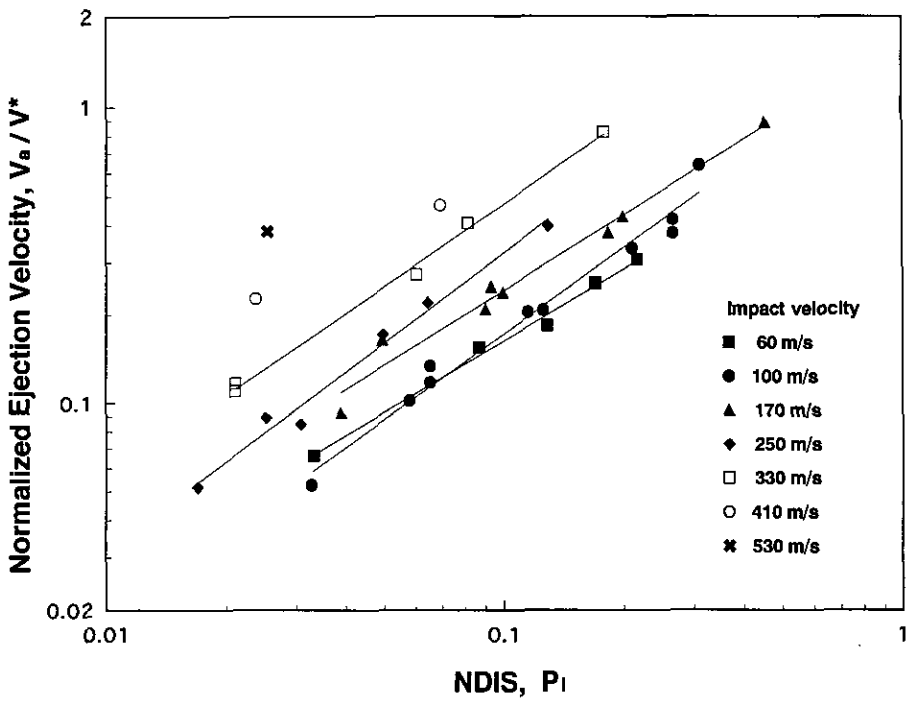

FIG. 5. Normalized ejection velocity vs nondimensional impact stress at a constant impact velocity. The data are fitted by the least-squares method and the resultant lines are also given.

sponding to $\bar{f}$ in Eq. (4) was not discussed by Mizutani *et al.* in detail. Since it highly depends on the shock-wave form at an antipodal point, it is usually difficult to evaluate an exact value of a for any case. According to a late-stage equivalence proposed by Dienes and Walsh (1970) and a late-stage effective energy proposed by Mizutani *et al.* (1990), the wave form should be almost the same on the far side from the impact point when the late stage effective energy of the projectile is equivalent at impact. Therefore, if the late-stage equivalence applies in our experiment, the value of a should be constant in any case. Thus, it is necessary to reconsider the scaling parameter P_I on the basis of two experimental results: the mass ratio dependence (log m_l/M_t) of log P_I, and the impact velocity dependence (log V_a/V^*) of log P_I. In the definition of P_I, the decay constant α is uncertain as discussed above. Next, we investigate the constant on the basis of experimental results for the ejection velocity.

5. DISCUSSION

In our experiment, the cone- and catastrophic-type disruptions have occurred. The former was also found in lower-velocity collisions of basalt targets (Fujiwara *et al.* 1989). Mizutani's theory for the ejection velocity is based on the idea of Rinehart (1975); it could be applicable to the spall fragment usually produced in the core and the catastrophic-type disruption at the rear. In the cone type disruption, the spalling could not be observed at the rear, so the constant a could not be determined by Eq. (5). In order to estimate the constant a, we simply assume $V_a \approx u_{fs}$(u_{fs} is the particle velocity at the antipodal point) for the catastrophic disruption. The pressure at the antipodal point is given by Eq. (2). When this pressure is low enough to ignore entropy effects (e.g., Duvall and Fowles 1963), for example 300 MPa for ice, and the free-surface approximation holds, the pressure is written using Eq. (3) as

$$P(L_t) = \rho_0 C_{0t} \frac{u_{fs}}{2}, \tag{10}$$

where C_{0t} is the bulk sound velocity of the target material and u_{fs} is the free-surface velocity. Equation (10) is rewritten by using V^* and the mass ratio of projectile to target as

$$\frac{V_a}{V^*} = 2P_I, \tag{11}$$

where

$$P_I = \frac{P_0}{Y_t}\left(\frac{m_p}{M_t}\right)^{\alpha/3}. \quad (12)$$

When this simple relation (11) is assumed, the decay constant α can be determined for each impact result in our experiments because the fragments with m_l/M_t lower than 0.1 were mostly formed by the catastrophic disruption; the data for such small fragments could be used for the analysis using Eq. (11). The result of the analysis is shown in Table I and Fig. 6. The calculated results using the data with m_l/M_t greater than 0.1 are also given in the table for reference and put in parentheses. The relation between n ($n \equiv \alpha/3$) and m_p/M_t at constant impact velocities is plotted in this figure. The value of n ranges from 0.7 to 1.2. It slightly increases as the mass ratio is close to unity at lower impact velocities; however, more data points for a wide range of the mass ratio at each impact velocity are necessary to determine the mass-ratio dependence of n. Although pressure decay has been reported to depend on both impact velocity and distance from impact point, i.e., mass ratio of projectile to target (Ahrens and O'Keefe 1977; Kieffer and Simonds 1980), the mass-ratio dependence was not confirmed in this study. Thus, n is assumed constant at a constant impact velocity in this analysis. The negative dependence of n on the impact velocity means that the impact pressure decays more slowly at a higher-velocity impact. The relation is clearly shown in Fig. 7, in which n is plotted against the impact velocity. This relation is represented by the following quadratic function at the impact velocities of 50–500 m/sec,

$$n = 1.20 - 1.38 \times 10^{-3} V_i + 6.18 \times 10^{-7} V_i^2. \quad (13)$$

These results clarified that the unrealistic assumption of $n = 1$ might be responsible for the target-size dependence of the largest fragment found in Fig. 3.

Figure 8 shows the relation between m_l/M_t and P_I^*, which is the modified nondimensional impact stress with the variable exponent n. The basalt data compiled by Takagi *et al.* (1984) are also shown for comparison. The variable n used to estimate the line for the basalt is assumed to be a constant equal to 1, because there was no apparent mass-ratio dependence on the largest fragment when P_I with a decay constant $\alpha = 3$ is used for the scaling parameter. Figure 8 is very different from Fig. 3 and clearly shows that the data points fall in a fairly narrow band irrespective of the mass ratio from 0.1 to 0.0015. P_I^* is a useful parameter to represent the largest fragment. The data in Fig. 8 can be fitted by

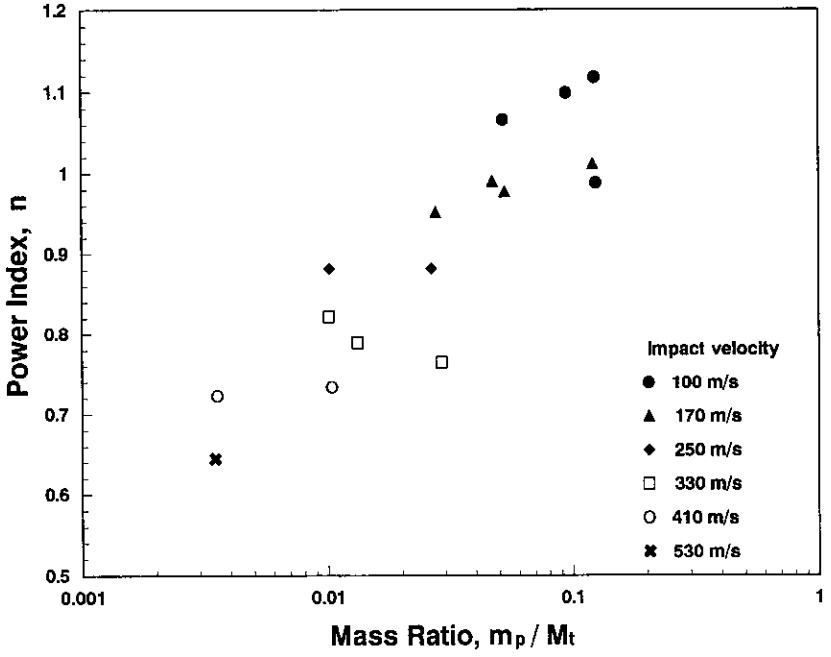

FIG. 6. Power index n ($n \equiv \alpha/3$) vs mass ratio at a constant impact velocity. n is calculated by Eqs. (11) and (12) for each raw data set with m_l/M_t lower than 0.1.

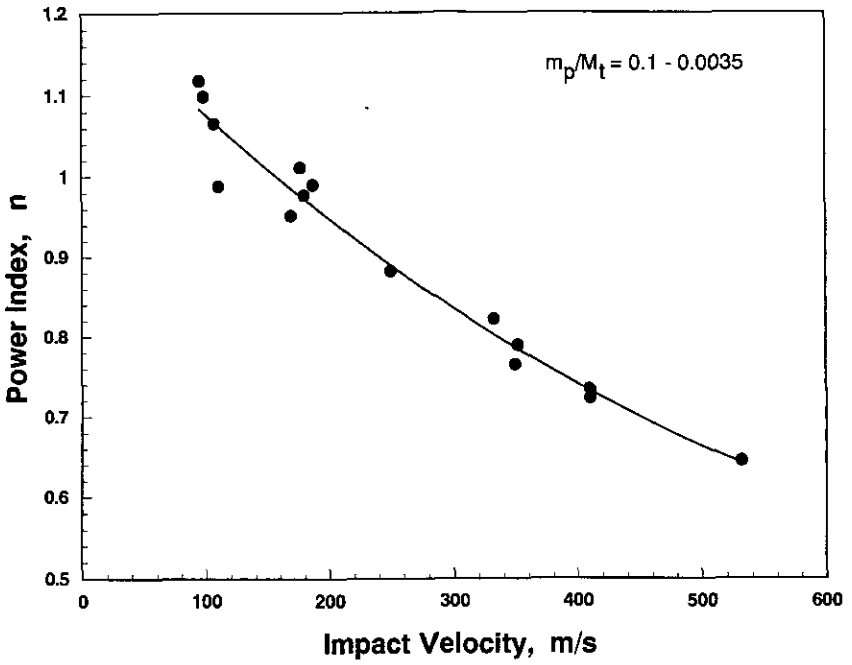

FIG. 7. Power index n vs impact velocity at m_l/M_t lower than 0.1. n could be fitted by a quadratic equation shown by the solid line.

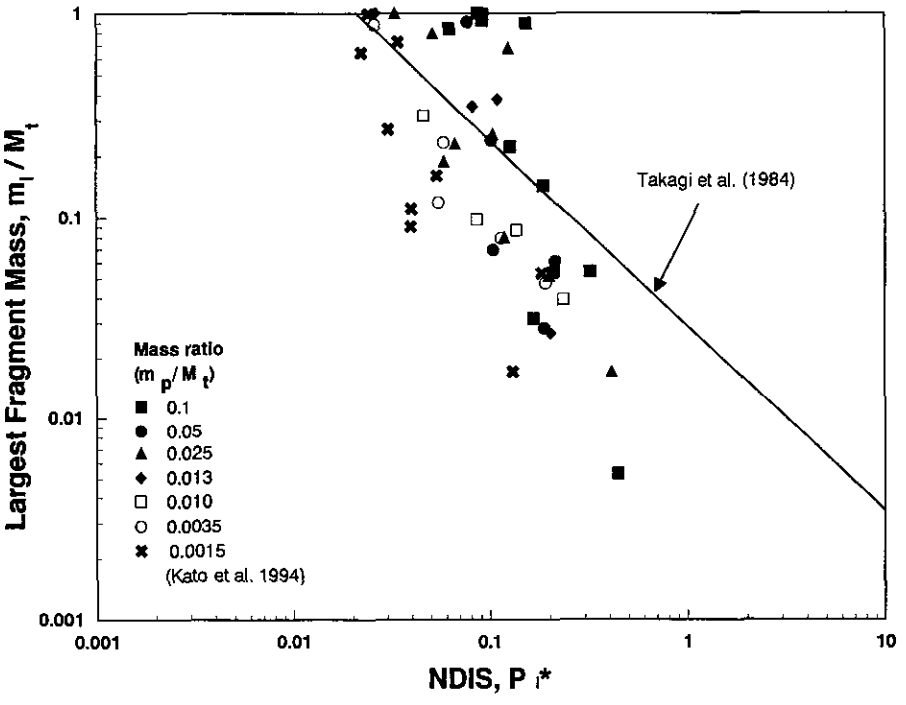

FIG. 8. Largest-fragment mass vs nondimensional impact stress with variable decay constant n at a constant mass ratio. Basalt data compiled by Takagi *et al.* (1984) are shown by a solid line; the nondimensional impact stress for the basalt used here is calculated by putting $n = 1$.

$$\frac{m_l}{M_t} = 10^{-2.2\pm0.2} P_I^{*-1.5\pm0.2}. \quad (14)$$

Since the beginning of the breakup of a target is calculated with $m_l/M_t = 1$, P_I^* is 0.033. This is very close to 0.029 for basalt, while the power index for ice is smaller than -0.92 for basalt. This comparison shows that ice could break into smaller pieces than basalt with an increase of the nondimensional impact stress.

We estimate the condition for an accretion of fragments by using our results obtained for the ejection velocities. Fragments are captured by planetary gravity depending on their ejection velocities. This gravitational capture of fragments after the collisional disruption is an important phenomenon for the planetary accretion and the origin of asteroids. The gravity of the planet must be considered for simulating the planet collision, thus V_a in the laboratory reference frame must be changed to the ejection velocity in the center-of-mass frame (V_{a-c}). V_{a-c} is defined as the differential velocity between V_a and the velocity of the center-of-mass, and written by using Eq. (11) as

$$V_{a-c} = V_a - V_c = 2V^* \frac{P_0}{Y_t} \left(\frac{m_p}{M_t}\right)^n - \frac{m_p/M_t}{1 + (m_p/M_t)} V_i, \quad (15)$$

where V_c is the velocity of the center-of-mass. When Eq. (6) is substituted into V^*, this equation is independent of the target strength, Y_t. Therefore, it is not necessary to consider the target-size dependence proposed by Housen and Holsapple (1990) for Y_t on the ejection velocity when the equation is applied to large planets. The calculated V_{a-c} using Eq. (15) is presented in Fig. 9 against the mass ratio at constant impact velocities, and this figure shows good agreement with the experimental data. At low impact velocity of 100 m/sec, V_{a-c} is almost 0 m/sec at m_p/M_t lower than 0.01 and becomes negative near 0.05, which means that the antipodal point moves to the opposite direction of the incoming projectile in the center-of-mass frame. In the higher-impact velocity range of 170 to 410 m/sec, V_{a-c} gradually increases from 0 to 10 m/sec with increasing m_p/M_t. V_{a-c} at higher impact velocities is higher at the same m_p/M_t. Equation (15) with the empirical parameter n is useful to express V_{a-c} in our experimental range. V_{a-c} becomes 0 m/sec as m_p/M_t approaches 0 and V_{a-c} becomes $V_i/2$ as m_p/M_t is close to unity under the condition that P_0 is proportional to the particle velocity.

Figure 10 shows the calculated results of Eq. (15) for variable impact velocities in a wide range of V_{a-c}. For example, m_p/M_t would be 0.02 for V_{a-c} of 1 m/sec and 0.2 for V_{a-c} of 10 m/sec at the constant impact velocity of 200 m/sec. The calculation is extrapolated to the mass ratio of unity although our data ranged below 0.1. Fujiwara and Tsukamoto (1980) claimed that 70 to 80% by mass of fragments have ejection velocities lower than about twice the antipodal velocity for basalt. If we use their results for natural ice collision, the reaccumulation of fragments in the collision of icy planetesimals is considered as follows. We compare half the escape velocity of the icy planets ($\frac{1}{2} V_{esc}$), with radii of 5, 25, 50, and 100 km and density of 10^3 kg/m^3, with the ejection velocity in Fig. 10, where $\frac{1}{2}V_{esc}$ is shown by the dashed lines. For instance, when a planet with a radius of 5 km collides at 200 m/sec, planets with radii larger than 1.8 km could cause the reaccumulation of most fragments including antipodal ones. However, when a planet of 25-km radius collides with another planet smaller than 7 km at 400 m/sec, few fragments accrete on the surface.

The collisional condition for the gravitational reaccumulation of the major mass of fragments is shown in Fig. 11. The condition of gravitational reaccumulation for planets with radii from 5 to 100 km can be obtained from the contours in Fig. 11. These contours were calculated by setting $V_{a-c} = \frac{1}{2} V_{esc}$ in Eq. (15). In the region above each line, the gravitational reaccumulation is difficult for small high-velocity fragments splashing out from the gravitational field. In the region below the line, most of the fragments including the antipodal fragment could be captured by gravity. The critical value of m_p/M_t decreases with increasing impact velocity and the slope of the boundary between reaccumulation and escape becomes steeper as the radius is larger; thus the region of the reaccumulation rapidly becomes larger with increasing radius.

6. CONCLUSIONS

Ice-to-ice collisional experiments were made with a wide variety of mass ratios, from 0.1 to 0.0035, and impact velocities, from 30 to 540 m/sec, and the largest-fragment mass and the ejection velocity at the antipodal point of the target were measured. From the results, it was concluded that the ice target could break up into smaller pieces easily and the fragments were ejected with higher velocity than basalt at the same energy-density collision. The physical conditions of reaccumulation (mass, mass ratio, and impact velocity) for the icy planetesimals can be estimated from Fig.11, which was made by using Eq. (15) and the experimentally determined decay constant n. For example, at 50-km radius when m_p/M_t is smaller than 0.2, reaccumulation could occur at impact velocities lower than 300 m/sec. Planets with radius smaller than 5 km cannot capture fragments after collision at wide mass ratios (m_p/M_t) of $1-10^{-3}$ when the collision occurs at impact velocities higher than 400 m/sec. This figure is necessary to study kinematic processes in planetary reaccretion with impact disruption and the origin of asteroids, although the material dependence

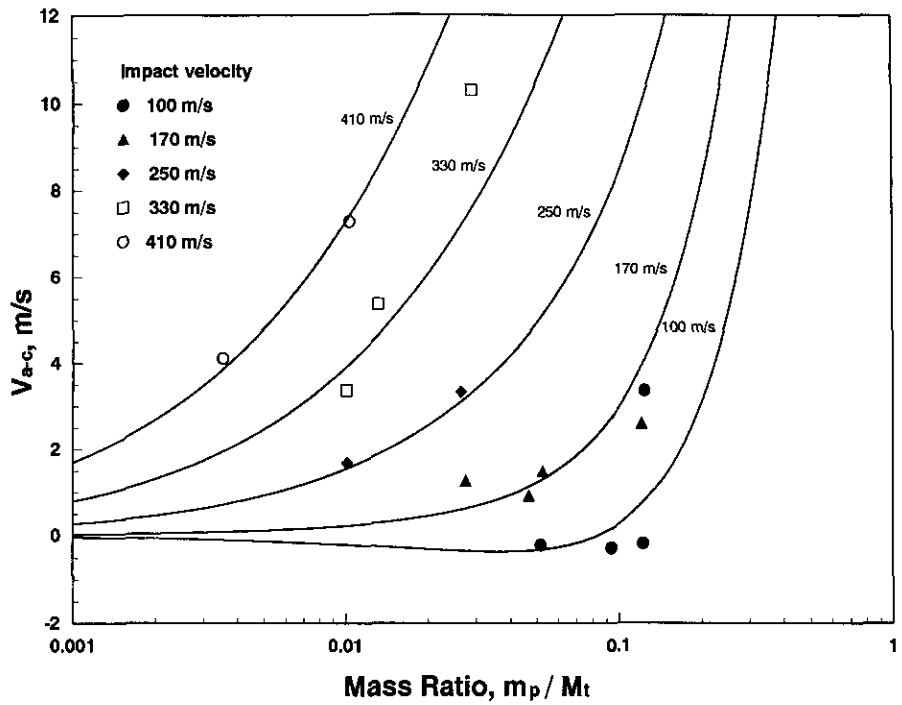

FIG. 9. Antipodal velocity in a center-of-mass frame vs mass ratio at a constant impact velocity. The thick solid lines were estimated from Eq. (15).

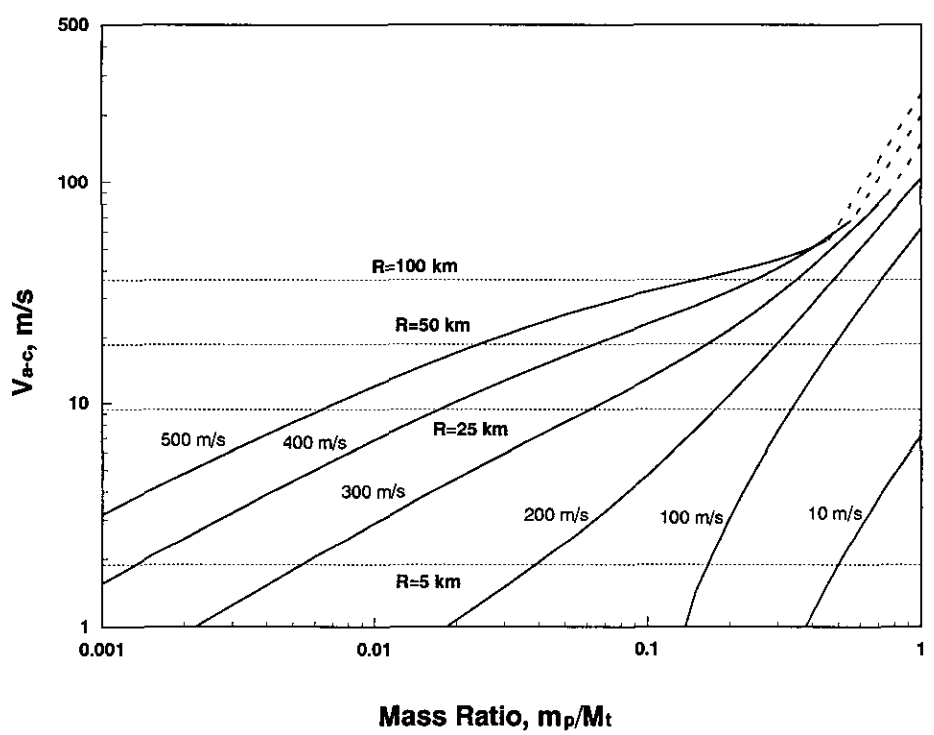

FIG. 10. Calculated antipodal velocity in a center-of-mass frame versus mass ratio. V_{a-c} is calculated by Eq. (15). Dashed lines refer to V_{a-c} which may be erroneous because the rear pressure may be larger than 300 MPa. Dotted lines are half of the escape velocities for an icy satellite of density 10^3 kg/m^3 and radii of 5, 25, 50, and 100 km.

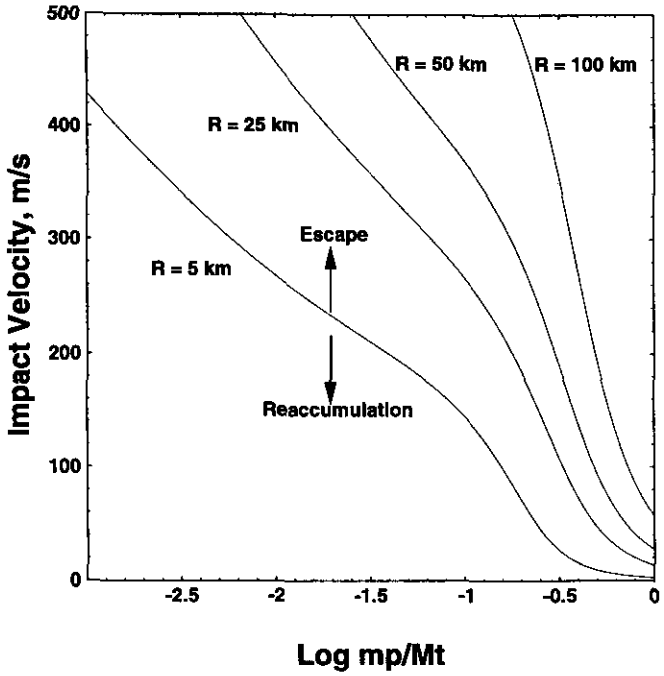

FIG. 11. Reaccumulation condition of fragments on various icy planets. Each of the lines gives the critical condition, whether most of the impact fragments including the largest fragment are captured by the planetary gravity (reaccumulation) or not (escape).

of the reaccumulation conditions for ice, rock, and metal, and the conditions for the higher-impact velocity should be examined in future work.

ACKNOWLEDGMENTS

We thank Dr. K. Nishimura of the Institute of Low Temperature Science, Hokkaido University for his help with the high-speed video camera, and Professor T. Yamamoto of the Department of Earth and Planetary Science, Hokkaido University and Professor H. Mizutani of the Institute of Space and Astronautical Science for their useful discussions and advice on the experimental results. We also appreciate greatly the technical help of T. Segawa and S. Nakatsubo of the Construction Division of the Institute of Low Temperature Science, Hokkaido University.

REFERENCES

AHRENS, T. J., AND J. D. O'KEEFE 1977. Equations of state and impact-induced shock wave attenuation on the Moon. In *Impact and Explosion Cratering* (D. J. Roddy, R. O. Pepin, and R. B. Merrill, Eds.), pp. 639–656. Pergamon, New York.

ARAKAWA, M., AND N. MAENO 1992. Mechanical deformation of polycrystalline ice I_h at temperatures 100K–263K: First report. In *Physics and Chemistry of Ice* (N. Maeno and T. Hondoh Eds.), pp. 464–469. Hokkaido Univ. Press, Sapporo.

BARGE, P., AND R. PELLAT 1993. Mass spectrum and velocity dispersions during planetesimal accumulation. II. Fragmentation. *Icarus* **104,** 79–96.

CINTALA, M. J., F. HÖRZ, S. SMREKAR, AND F. CARDENAS 1985. Impact experiments in H_2O ice, II; Collisional disruption. *Proc. Lunar Planet. Sci. Conf. 16th,* pp. 129–130, Lunar and Planetary Institute, Houston.

DAVIS, D. R., AND E. V. RYAN 1990. On collisional disruption: Experimental results and scaling laws. *Icarus* **83,** 156–182.

DIENES, J. K., AND J. M. WALSH 1970. Theory of impact: Some general principles and the method of Eulerian codes. In *High-Velocity Impact Phenomena* (R. Kinslow, Ed.), pp. 45–104. Academic Press, New York.

DUVALL, G. E., AND G. R. FOWLES 1963. Shock waves. In *High-Pressure Physics and Chemistry* (R. S. Bradley, Ed.), Vol. 2, pp. 209–291. Academic Press, New York.

FUJIWARA, A., G. KAMIMOTO, AND A. TSUKAMOTO 1977. Destruction of basaltic bodies by high-velocity impact. *Icarus* **31,** 277–288.

FUJIWARA, A., AND A. TSUKAMOTO 1980. Experimental study on the velocity of fragmentations in collisional breakup. *Icarus* **44,** 142–153.

FUJIWARA, A., P. CERRONI, D. DAVIS, E. RYAN, M. DI MARTINO, K. HOLSAPPLE, AND K. HOUSEN 1989. Experiments and scaling laws for catastrophic collisions. In *Asteroids II* (R. P. Binzel, T. Gehrels, and M. S. Matthews, Eds.), pp. 240–265. Univ. of Arizona Press, Tucson.

GAFFNEY, E. S. 1985. Hugoniot of water ice. In *Ices in the Solar System* (J. Klinger, D. Benest, A. Dollfus, and R. Smoluchowski, Eds.), pp. 119–148. Reidel, Dordrecht.

GOLD, L.W. 1958. Some observations on the dependence of strain on stress in ice. *Can. J. Phys.* **36,** 1265–1275.

HAYAKAWA, M., H. MIZUTANI, S. KAWAKAMI, AND Y. TAKAGI 1989. Numerical simulation of collisional accretion process of the earth. *Proc. Lunar Planet. Sci. Conf. 19th,* pp. 659–671.

HOUSEN, K. R., AND K. A. HOLSAPPLE 1990. On the fragmentation of asteroids and planetary satellites. *Icarus* **84,** 226–253.

KATO, M., Y. IIJIMA, Y. OKIMURA, M. ARAKAWA, N. MAENO, A. FUJIMURA, AND H. MIZUTANI 1992. Impact experiments on low temperature H_2O ice. In *Physics and Chemistry of Ice* (N. Maeno and T. Hondoh, Eds.), pp. 237–244. Hokkaido Univ. Press, Sapporo.

KATO, M., Y. IIJIMA, M. ARAKAWA, Y. OKIMURA, A. FUJIMURA, N. MAENO, AND H. MIZUTANI 1995. Ice-on-ice impact experiments. *Icarus,* **113,** 423–441.

KAWAKAMI, S., H. MIZUTANI, Y. TAKAGI, M. KATO, AND M. KUMAZAWA 1983. Impact experiments on ice. *J. Geophys. Res.* **88,** 5806–5814.

KIEFFER, S. W., AND C. H. SIMONDS 1980. The role of volatiles and lithology in the impact cratering process. *Rev. Geophys. Space Phys.* **18,** 143–181.

LANGE, M. A., AND T. J. AHRENS 1983. The dynamic tensile strength of ice and ice–silicate mixtures. *J. Geophys. Res.* **88,** 1197–1208.

LANGE, M. A., AND T. J. AHRENS 1987. Impact experiments in low-temperature ice. *Icarus* **69,** 506–518.

LARSON, D. B. 1984. Shock-wave studies of ice under uniaxial strain conditions. *J. Glaciol.* **30,** 235–240.

MELOSH, H. J. 1989. *Impact Cratering.* Oxford Univ. Press, New York.

MIZUTANI, H., Y. TAKAGI, AND S. KAWAKAMI 1990. New scaling laws on impact fragmentation. *Icarus* **87,** 307–326.

NAKAMURA, A., AND A. FUJIWARA 1991. Velocity distribution of fragments formed in a simulated collisional disruption. *Icarus* **92,** 132–146.

NAKAMURA, A., K. SUGIYAMA, AND A. FUJIWARA 1992. Velocity and spin of fragments from impact disruptions 1. An experimental approach to a general law between mass and velocity. *Icarus* **100,** 127–135.

RINEHART, J. S. 1975. *Stress Transients in Solids.* Hyper Dynamics, Santa Fe, NM.

TAKAGI, Y. 1983. *Fragmentaion experiments of basalt: Size and velocity distribution of fragments.* Master's thesis, Nagoya University.

TAKAGI, Y., H. MIZUTANI, AND S. KAWAKAMI 1984. Impact fragmentation experiments of basalts and pyrophyllites. *Icarus* **59,** 462–477.

WAZA, T., T. MATSUI, AND K. KANI 1985. Laboratory simulation of planetesimal collisions 2. Ejecta velocity distribution. *J. Geophys. Res.* **90,** 1995–2011.

WETHERILL, G. W., AND G. R. STEWART 1993. Formation of planetary embryos: Effects of fragmentation, low relative velocity, and independent variation of eccentricity and inclination. *Icarus* **106,** 190–209.